Materials Science and Engineering C 69 (2016) 1147–1158

Contents lists available at ScienceDirect

Materials Science and Engineering C

journal homepage: www.elsevier.com/locate/msec

In vitro evaluation of actively targetable superparamagnetic nanoparticles to the folate receptor positive cancer cells

Rozita Nasiri [a], Javad Hamzehalipour Almaki [a], Ani Binti Idris [a,*], Fadzilah Adibah Abdul Majid [a,e], Mahtab Nasiri [b], Mojtaba Salouti [c], Muhammad Irfan [a], Neda Amini [d], Mohsen Marvibaigi [d]

[a] Institute of Bioproduct Development, Department of Bioprocess and Polymer Engineering, Faculty of Chemical and Energy Engineering, Universiti Teknologi Malaysia, Skudai, 81310 Johor Bahru, Johor, Malaysia
[b] Advanced Materials Research Center, Department of Materials Engineering, Najafabad Branch, Islamic Azad University, Najafabad, Iran
[c] Biology Research Centre, Zanjan Branch, Islamic Azad University, Zanjan, Iran
[d] Faculty of Biomedical Engineering, Universiti Teknologi Malaysia, Skudai, 81310 Johor Bahru, Johor, Malaysia
[e] Institute of Marine Biotechnology, Universiti Malaysia Terengganu, 21300 Kuala Terengganu, Terengganu, Malaysia

ARTICLE INFO

Article history:
Received 12 November 2015
Received in revised form 16 July 2016
Accepted 30 July 2016
Available online 1 August 2016

Keywords:
Co-precipitation
Bioconjugation
Targeting
Superparamagnetic
Iron oxide nanoparticles
FAR+ cancer cells

ABSTRACT

Engineering of a physiologically compatible, stable and targetable SPIONs-CA-FA formulation was reported. Initially fabricated superparamagnetic iron oxide nanoparticles (SPIONs) were coated with citric acid (CA) to hamper agglomeration as well as to ameliorate biocompatibility. Folic acid (FA) as a targeting agent was then conjugated to the citric acid coated SPIONs (SPIONs-CA) for targeting the specific receptors expressed on the FAR+ cancer cells. Physiochemical characterizations were then performed to assure required properties like stability, size, phase purity, surface morphology, chemical integrity and magnetic properties. *In vitro* evaluations (MTT assay) were performed on HeLa, HSF 1184, MDA-MB-468 and MDA-MB-231cell lines to ensure the biocompatibility of SPIONs-CA-FA. There were no morphological changes and lysis in contact with erythrocytes recorded for SPIONs-CA-FA and SPIONs-CA. High level of SPIONs-CA-FA binding to FAR+ cell lines was assured via qualitative and quantitative *in vitro* binding studies. Hence, SPIONs-CA-FA was introduced as a promising tool for biomedical applications like magnetic hyperthermia and drug delivery. The *in vitro* findings presented in this study need to be compared with those of in vivo studies.

1. Introduction

Nowadays, development of specific, highly sensitive and rapid detection methods for cancer diagnosis is crucial because cancer has become a major public concern and inadequate typical treatments are applied [1,2]. Recent nanotechnological advances offer platforms to fabricate ultrasmall probes like superparamagnetic iron oxide nanoparticles. SPIONs are well known for their invaluable function in biomedical applications like magnetic resonance imaging (MRI),intracellular magnetic hyperthermia, targeted drug delivery, cell tracking and labelling, localized therapy, etc. [3,4]. Currently, SPIONs are in preclinical studies as well as in early stage clinical trials [3,5]. A variety of methods have been reported to synthesize SPIONs like micro emulsion, sono-chemical synthesis, thermal decomposition, hydrothermal synthesis, co-precipitation, etc. [6,7]. But, co-precipitation is a neat and suitable method for synthesis of SPIONs smaller than 20 nm in diameter [8]. Desired SPIONs for various biomedical applications are between 10 nm and 100 nm in diameter [9]. Recent investigations have reflected the fact that SPIONs are highly favorable drug targeting platforms because of their rather poor toxic effects [10] and high magnetic saturation magnitudes [11].

However, due to the hydrophobic nature of SPIONs, they are instable and prefer to aggregate in physiological condition [12,13]. Moreover, the large surface area to volume ratio of SPIONs compels the tendency to aggregate thus limiting their naturally high level of surface energy [14]. Therefore, organic or inorganic materials are used to coat the SPIONs surface to barricade agglomeration and ensure biocompatibility. Coating not only stabilizes the SPIONs, but also promotes the attachment of biological moieties to them; the particles are targeted to cells by attaching functional groups to the SPIONs. Citric acid ($C_6H_8O_7$) has been extensively used as a biocompatible and short-chained tri-carboxylic acid to stabilize SPIONs for different biomedical applications [15–17].

Since high level of targeting is not offered by SPIONs due to their physiochemical profiles, active biomolecules are attached to the surface of the SPIONs to heighten the targeting specificity of nanoparticles [5,18,19]. Clinical utility of the SPIONs is significantly increased after

* Corresponding author at: Department of Bioprocess Engineering, Faculty of Chemical Engineering c/o Institute of Bioproduct Development, Universiti Teknologi Malaysia, Skudai, 81310 Johor Bahru, Johor, Malaysia.
E-mail address: ani@cheme.utm.my (A.B. Idris).

http://dx.doi.org/10.1016/j.msec.2016.07.076
0928-4931/

being bonded to the contrast agents allowing the SPIONs to accumulate in the sites of interest [20–22]. Additionally, various studies have pointed out diverse approaches for active targeting of SPIONs by protein structures, nutrients and therapeutics. Internalization of structures attached to the SPIONs are inhibited due to the bulky and immunogenic nature of antibodies [23]. Since nutrient pathways increase the uptake of SPIONs because of their direct linkage to cell proliferation process, most tumor types provide signals more excellently. Tumor cells are dependent to folic acid (FA) as it is one of the essential precursors in synthesis of DNA base [24–26], In normal cells, folate receptors are slightly expressed [26]. Thus, it assists the nanoparticles conjugated with FA to be internalized to the cancer cells simultaneously expressing folate receptors (FAR+) through receptor-mediated endocytosis pathway due to high levels of penetration and affinity [27]. In most of the studies mentioned, folic acid was used in combination with nanostructures other than citrate-coated maghemite. But, in this study, folic acid was conjugated to the SPIONs via the help of citric acid resulting in synthesis of a novel biomaterial with a monodisperse nature and desired characteristics offering targeting capabilities to track and attach to the FAR+ cancer cells while being highly blood compatible and remarkably reduced cytotoxicity. In this research, to make the surface of the synthesized nanoparticles (γ-Fe_2O_3) hydrophilic, functional groups for further surface functionalization were provided, nanoparticles agglomeration was prevented and absorption of citric acid onto the surface of nanoparticles was carried out leaving a carboxylic acid exposed on the surface. The final product was engineered by conjugation of FA to the SPIONs-CA and it was physically and chemically characterized by a variety of evaluation and assessment methods. Stability, biocompatibility and binding response of the final exquisite engineered SPIONs-CA-FA were investigated *in vitro*.

2. Experimental section

2.1. Materials

Chemicals used in this study were of analytical purity and they are as follows: sulfuric acid (H_2SO_4) (QRëC), iron (II) chloride ($FeCl_2$) (99% purity, Sigma-Aldrich), iron (III) chloride ($FeCl_3$) (45% purity, Riedel-de Haen), acetone (QRëC), hydrochloric acid (HCl) (37% purity, QRëC), Folic acid (Sigma-Aldrich), potassium bromide (KBr, Sigma-Aldrich), N-ethyl-N-(3- dimethylaminopropyl) carbodiimide hydrochloride (EDC, 99% purity, Sigma-Aldrich), N-hydroxysuccinimide (NHS, 98% purity, Sigma-Aldrich), Bovine Serum Albumin (BSA, Sigma-Aldrich), Bradford Reagent (Sigma-Aldrich), human red blood cells (HRBCs), HSF 1184 cell line (Human skin fibroblast cell line, ATCC Manassas, VA), HeLa cell line (Human cervical cancer cell, ATCC Manassas, VA), MDA-MB-468 cell line (Human breast cancer cell, ATCC Manassas, VA), MDA-MB-231 cell line (Human breast cancer cell, ATCC Manassas, VA), fetal bovine serum (Gibco, USA), Trypsin EDTA (Gibco, USA), phosphate buffered saline (PBS, Gibco, USA), MES Sodium Salt (MES, Sigma-Aldrich), Dulbecco's modified Eagle's medium (DMEM, Gibco, USA), RPMI Medium 1640 (Gibco, USA), Penicillin-streptomycin (Gibco, USA), Dimethyl sulfoxide (DMSO, Sigma-Aldrich, Thiazolyl Blue Tetrazolium Bromide (MITT, Sigma-Aldrich), Prussian blue test kit (Sigma-Aldrich). In all the experiments, water was previously deionized (18 MΩ). All other chemicals were purchased from Sigma-Aldrich in analytical purity and were used without further purification.

2.2. Initial ferrofluids synthesis (γ-Fe_2O_3)

SPIONs (γ-Fe_2O_3) were fabricated using the protocol by Massart [28] and amended by Idris et al. [29] in which SPIONs superficial charge and size were controlled. Fabrication of SPIONs was accomplished via alkaline co-precipitation in that ferrous ($FeCl_3$) and ferric chloride ($FeCl_2$) were mixed stoichiometrically in a solution of ammonium hydroxide (NH_4OH) followed by acidification of precipitate (Fe_3O_4) by nitric acid (HNO_3) reversing surface charge and finally oxidized into maghemite (γ-Fe_2O_3) in ferric nitrate ($Fe(NO_3)_3 \cdot 9H_2O$) solution at 100 °C.

2.3. Citrate coating of SPIONs

The SPIONs were incubated with 0.5 g/ml citric acid solution for 1 h. The reaction was completed in 90 min at 90 °C. The mixture temperature was allowed to cool to room temperature where black precipitates were acquired and was further processed by washing with acetone to obtain citric acid coated SPIONs (SPIONs-CA) [30].

2.4. Folic acid conjugation

FA Conjugation to the SPIONs-CA was carried out via the EDC/NHS click chemistry reactions [31,32,33]. In brief, 1.2 mg (10 mmol) N-hydroxysuccinimide (NHS) and 0.6 mg (3 mmol) EDC were mixed and subsequently dissolved in 125 μl MES buffer (0.5 M, pH = 6.3) and added to 500 μl of SPIONs-CA and shaken for 1.5 h at room temperature. The mixture was washed twice with phosphate buffer solution (PBS), pH = 7.4 and magnetic separation technique was performed. The activated SPIONs-CA were mixed with 1 ml of folic acid (22 mg/ml) and agitated for 3 h. Then, 100 μl (25 mmol) glycine in PBS was added to the solution for 30 min while stirring so as to quench the reaction. Finally, SPIONs-CA-FA was centrifuged and washed with PBS several times.

2.5. Determination of folic acid loading content using high performance liquid chromatography (HPLC)

Determination of FA concentration in SPIONs-CA-FA was determined via HPLC ensuring the conjugation was performed well. The separation by HPLC was accomplished via Microsorb-MV C18 analytical column (250 mm × 4.6 mm I.D., 5 μm particle diameter, Varian Chromatographic Systems, Walnut Creek, CA) with a UV/VIS detector. Phosphoric acid 5% (phase A) and acetonitrile (ACN) (phase B) were utilized as eluents and the flow rate was kept at 0.8 ml/min. Results were recorded at a wavelength of 210 nm. The elution applied was as it follows: 0 min (100% buffer), 0–10 min gradient to a 90% buffer, 10–17 min isocratically 90% buffer, in 18th min 100% buffer and 18–25 min 100% buffer. According to the comparison between reference standards and retention times of the samples, identification of FA was performed. Folic acid reference solutions were made in different concentrations ranging from 50 to 1000 μg/ml for qualitative analysis in which every standard solution was analyzed with HPLC – UV/VIS three times. Efficiency of the conjugation was examined via Eq. (1).

$$\eta_{con}(\%) = \frac{M_{Hf}}{M_{Hi}} \times 100 \quad (1)$$

Where η_{con} represents conjugation efficiency, M_{Hf} is the amount of folic acid in ferrofluids suspension and M_{Hi} is the initial amount of folic acid.

2.6. Analytical methods

2.6.1. Assessing the size of samples

Transmission Electron Microscopy (TEM) was used to determine the size of samples. 5 μl of each of the samples (SPIONs, SPIONs-CA and SPIONs-CA-FA) was set down on a carbon grid. 5 μl of 1% phosphotungstic acid was added to the samples and mixture was allowed to settle for 30 s, negative staining was performed. Carbon grid was cleared from the liquid. Finally, the grid was scanned via a Hitachi H-7500 transmission electron microscope and the snapshots were then studied for approximate determination of samples' diameters.

2.6.2. Morphology of samples

Field Emission Scanning Electron Microscopy (FESEM) was used to analyze the morphology of SPIONs, SPIONs-CA and SPIONs-CA-FA. The snapshots were taken using FESEM (JSM-6700F, JEOL, Tokyo, Japan) operating at accelerating voltage of 5 kV and working distance of 1.5 cm between the detector and the samples. The samples were prepared where sample suspension (a droplet) was placed on a copper tape stuck to the stub. Then, the sample droplet was air-dried prior to be coated via platinum coater (30 mA, 30 s).

2.6.3. Structural analysis

Fourier Transform Infrared Spectroscopy (FTIR) was used to analyze the chemical integrity of CA and FA after CA coating and FA conjugation, respectively. By applying a pressure of 300 kg/cm^2, the samples were crushed with KBr to obtain the pellets. The FTIR spectra of SPIONs, CA, SPIONs-CA, FA and SPIONs-CA-FA were scanned in the range of 400–4000 cm^{-1}.

2.6.4. Determination of hydrodynamic diameter

Dynamic Light Scattering (DLS) was used to measure the hydrodynamic diameter of the samples (neat SPIONs, SPIONs-CA and SPIONs-CA-FA). Each sample (100 μl) was diluted by 4 ml of MiliQ water (<0.2 mg/ml). Cellulose acetate membrane (0.45 μm) was used to filter the samples into cuvettes. Then, filtrates were transferred to low-volume quartz cuvettes to be examined via a ZetaSizerNano ZS90 particle-sizing instrument (Malvern, Worcestershire, UK). Samples were then equilibrated at 25 °C for 5 min prior to each of the measurements. The stability, particle size distribution of the samples and polydispersity index (PDI) were measured in which data were collected for 15 min and the process was repeated six times.

2.6.5. Iron concentrations of the samples

Atomic Absorption Spectroscopy (AAS) was used to compute the iron concentrations of the samples at 248.3 nm (SpectrAA-10 Plus spectrometer, Varian, France). Each sample suspension (1 ml) was digested by 5 ml of HCL (6 M) overnight before the AAS. The resultant solution was then diluted with 1% hydrochloric acid. Generation of the calibration curve was carried out by treating an $FeCl_3$ acidic solution (Titrisol standard solution, 2 g/l) under the same conditions [34].

2.6.6. Assessment of magnetic properties

The magnetic properties of SPIONs, SPIONs-CA and SPIONs-CA-FA were assessed using a Lakeshore 7307 (Lakeshore Cryotronic) vibrating sample magnetometer (VSM) at 300 K.

2.6.7. Crystallinity structure

X-Ray Diffraction (XRD) was used to determine and verify the crystalline structure of SPIONs, SPIONs-CA and SPIONs-CA-FA. The Panalytical X'PERT MPD X-ray diffractometer was equipped with a copper anode generating high intensity Cu Kα radiation ($\lambda = 1.54065$ Å) with the 2θ range from 10° to 90°.

2.7. In-vitro analysis

2.7.1. Cell line

The HSF 1184, HeLa, MDA-MB-468 and MDA-MB-231 cell lines were procured from ATCC. The HSF 1184, MDA-MB-231 and MDA-MB-468 cell lines were cultured in DMEM medium supplemented with 10% fetal bovine serum (VWR, Visalia, CA) and 1% penicillin–streptomycin (Sigma, St. Louis, MO). HeLa cells were cultured in RPMI 1640 medium with 10% fetal bovine serum (VWR, Visalia, CA) and 1% penicillin–streptomycin (Sigma, St. Louis, MO). Cells were grown at 37 °C in a humidified atmosphere of 5% CO_2 (v/v) in air. All experiments were followed out in the exponential growth phase of the cells.

2.7.2. In vitro RBC, WBC and PRP aggregation; and haemolysis studies

For haemolysis study, 900 μl (100, 200 and 300 μg/ml in saline) of each of the samples (SPIONs, SPIONs-CA and SPIONs-CA-FA) was diluted with 100 μl of washed RBCs and allowed to incubate for 2 h. The samples were then centrifuged (5 min, 1500 rpm) and subsequently, 900 μl of saline was added to the supernatant and the absorption was recorded at 541 nm using UV spectrophotometer (Carywin UV). Saline and water were used as negative control and positive controls respectively. Visual assessment of the aggregation through phase contrast microscope (Leica DM IRB, Germany) was performed by adding 50 μl of SPIONs, SPIONs-CA and SPIONs-CA-FA to 100 μl of diluted RBCs, WBCs and platelet-rich plasma (PRP) which were then located in 37 °C incubator for 30 min. Saline and Triton X-100 was used as negative and positive controls respectively [35]. The percentage of haemolysis was determined using Eq. (2).

$$\%\text{of haemolysis} = \frac{\text{OD sample} - \text{OD }(-)\text{control}}{\text{OD }(-)\text{control} - \text{OD }(+)\text{control}} \times 100 \quad (2)$$

2.7.3. Cell compatibility study

Tetrazolium dye (MTT) assay was performed in order to evaluate the viability of HSF 1184, HeLa, MDA-MB-468 and MDA-MB-231 cell lines in contact with SPIONs, SPIONs-CA and SPIONs-CA-FA [36]. Cells were harvested and resuspended at 5×10^4 cells/200 μl in their related medium (supplemented with 10% fetal bovine serum and 1% penicillin-streptomycin). Then, the cells were cultured in 24-well plates. Subsequently, after 24 h, the medium of each cell line was replaced with 200 μl of each sample (7.8, 15.62, 31.25, 62.5, 125, 250, 500, 1000 μg/ml) diluted with medium and located in incubator for 24 h. Then, to each well, 20 μl of MTT (5 mg/ml) was added and cells were further incubated for another 4 h in a dark area as it is a light sensitive reaction. Then, the process was followed up by aspirating off the formulations and addition of DMSO (200 μl) to dissolve the formazan crystals. Later, absorbance was measured at 570 nm via a BioRad microplate reader. Untreated cells and medium were used as controls with 100% viability and blank respectively. Finally, results were expressed as mean values ± standard deviation of 6 independent measurements. The relative cell viability (%) compared to the control group was obtained via Eq. (3).

$$\text{cell viability }(\%) = \frac{\text{OD 570 (sample)}}{\text{OD 570 (control)}} \times 100 \quad (3)$$

2.7.4. Quantitative binding study

The HSF 1184, HeLa, MDA-MB-468 and MDA-MB-231 cell lines were seeded in 4-well plates (5×10^4 cells/well) at 37 °C in their related mediums (supplemented with 10% fetal bovine serum and 1% penicillin-streptomycin) until reaching 70–90% confluence. Cell lines were treated with SPIONs-CA and SPIONs-CA-FA suspensions (concentration of iron content: 100 μg/ml, 200 μg/ml and 300 μg/ml) for 4, 12 and 24 h incubated at 37 °C in order to evaluate the cell binding properties of the samples. Unbound nanoparticles were eliminated by washing with PBS (pH 7.4) three times at regular time intervals. Highly concentrated HCl was used to digest the cells during 48 h. Finally, via AAS, the iron content of the cell lyzate was studied. The average result was calculated from six samples [34].

In order to determine whether folate ligands mediated the cellular uptake of SPIONs-CA-FA specifically, the competitive binding experiments were carried out. Therefore, SPIONs-CA-FA (250 μg/ml, 24 h) underwent a co-incubation with free folic acid (1 mM) in HSF 1184, HeLa, MDA-MB-468 and MDA-MB-231 cell lines. In these experiments, folate receptors were saturated in order to restrict the receptor-specific binding by SPIONs-CA-FA that assisted the distinguishing between non-specific nanoparticles and receptor-mediated cellular uptake [37].

2.7.5. Qualitative binding study

Determination of the cellular uptake of iron in different cell lines was performed using Prussian blue staining method. The HSF 1184, HeLa, MDA-MB-468 and MDA-MB-231 cell lines were seeded in 4-well plates (5×10^4 cells/well) at 37 °C in their related mediums (supplemented with 10% fetal bovine serum and 1% penicillin-streptomycin) until a confluence of 70–90% was achieved. Later, the cells were treated with SPIONs-CA and SPIONs-CA-FA suspensions (concentration of iron content: 100 μg/ml and 200 μg/ml) and incubated at 37 °C for 24 h. Cells were then fixed in a 4% formaldehyde/PBS solution (pH 7.4) for 30 min prior to staining the cells with Prussian blue staining kit according to the instruction protocols. Images were then scanned via light microscope (Olympus, Fluoview FV1000 Microscope, Japan).

2.8. Statistics

GraphPad Prism software (version 6.0) was used to analyze the data and the results were expressed as mean ± S.E.M. of at least three independent experiments. One or two-factor ANOVAs with appropriate post-tests as well as the multiple t-test analysis were performed as illustrated in the result section. Data with p-value < 0.05 were considered statistically significant.

3. Results and discussion

3.1. Synthesis and characterizations

Fig. 1a illustrates the schematic presentation of SPIONs-CA-FA binding to the folate receptor positive cancer cells. The exquisite SPIONs-CA-FA fabricated as a stable and biocompatible targeting material contains exposed hydroxyl groups on the surface. Initially the SPIONs surface was coated with CA via method of direct addition and the obtained SPIONs are expected to contain exposed carboxylic groups on the surface (Fig. 1b (A)).

Finally, conjugation of FA through EDC/NHS click chemistry method was accomplished (Fig. 1b (B1, B2)). The HPLC results indicated 50% efficiency of FA conjugation to the active carboxylate group on the surface of nanoparticles. In Fig. 2, TEM and FESEM micrographs depict that the size distribution and spherical morphology of the SPIONs, SPIONs-CA and SPIONs-CA-FA are nearly uniform. The size of the SPIONs with a dominant population around 10–11 nm is shown in Fig. 2(b). From TEM and FESEM images (Fig. 2), the bare SPIONs were seen to exhibit agglomeration. All the particles were observed to be spherical in shape and seemed to have smooth surface within the FESEM resolution level. Citrate ions were used as an interfacial layer to make the produced maghemite nanoparticles compatible for biomedical application and to

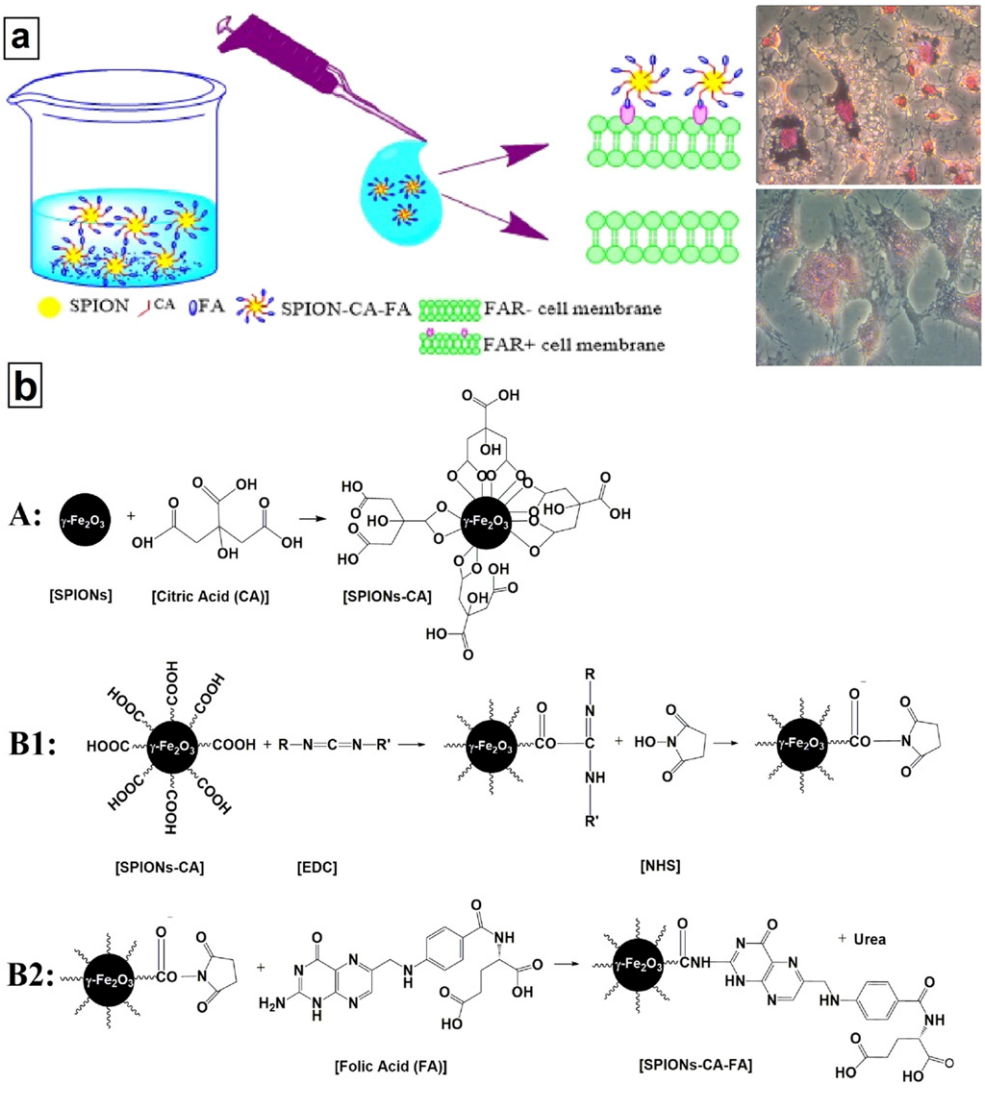

Fig. 1. a) Schematic presentation of SPIONs-CA-FA binding to the FAR+ cancer cells, b) synthesis route of citric acid coating (A), conjugation activation (B1) and FA conjugation (B2).

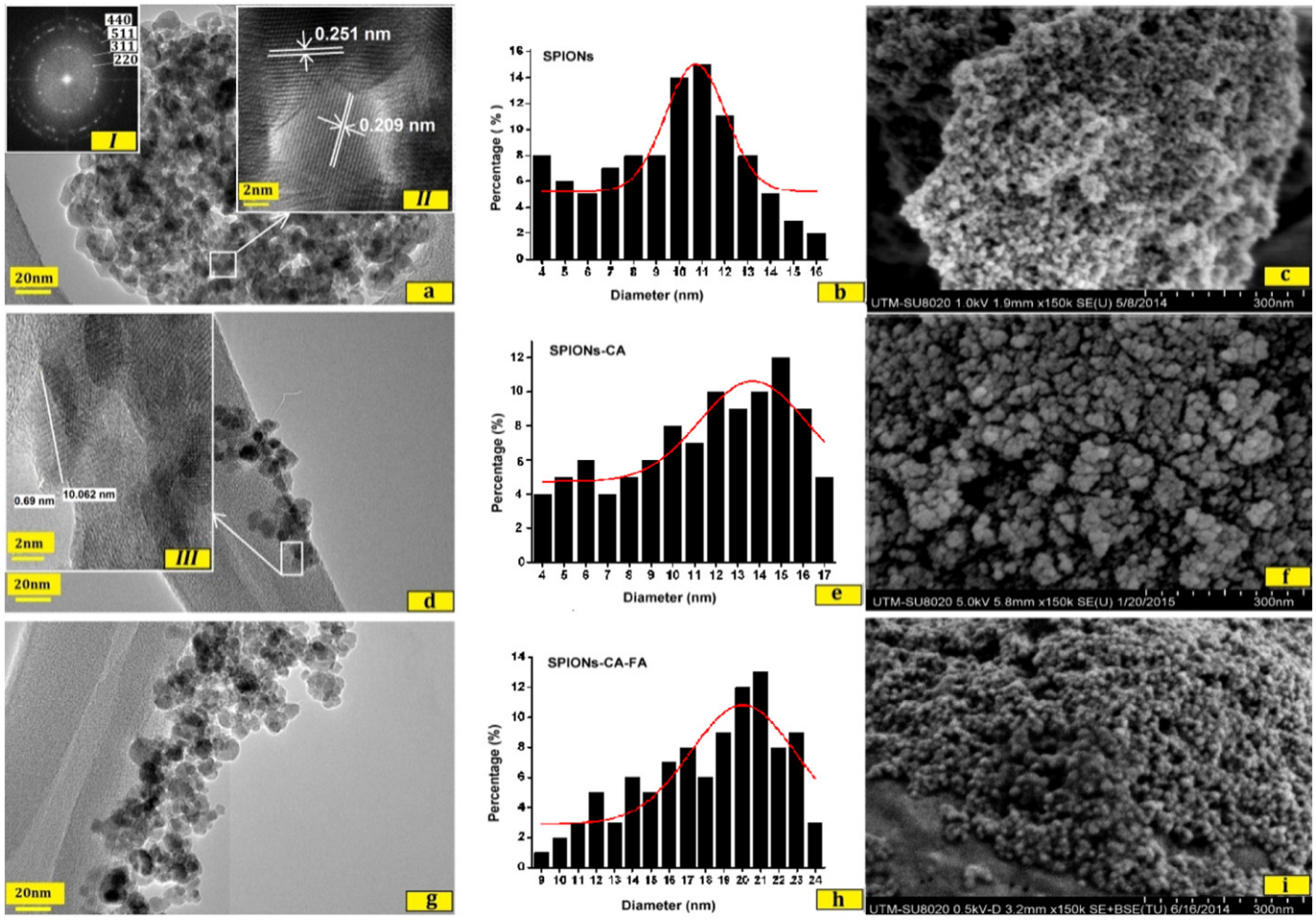

Fig. 2. a) TEM images of bare SPIONs, SAED patterns (I) and HRTEM (II) of SPIONs, b) SPIONs average size, c) FESEM image of bare SPIONs, d) TEM images of SPIONs-CA and HRTEM core–shell structure of CA-SPIONs (III) e) SPIONs-CA average size, f) FESEM image of SPIONs-CA, g) TEM images of SPIONs-CA-FA, h) SPIONs-CA-FA average size, i) FESEM image of SPIONs-CA-FA.

achieve carboxylic active sites on the surface of SPIONs. The SPIONs-CA were observed to be slightly bigger than bare SPIONs (Fig. 2(c)) about 12–15 nm diameters and showed less agglomeration compared to the SPIONs as shown in FESEM images (Fig. 2(f)).

The typical core–shell structure of CA-SPIONs (Fig. 2(d)) and thin layer of CA is observed on the γ-Fe_2O_3 core. The thickness of the CA layer was repeatedly calculated to determine its value which was found ranging from 0.2–0.5 nm (Fig. 2(d *(III)*). The selected area electron diffraction (SAED) patterns represent the crystallinity of SPIONs aggregates (Fig. 2(a *(I)*). The high-resolution transmission electron micrograph (HRTEM) (Fig. 2(a *(II)*) shows high crystallinity of the SPIONs with lattice spacing of 0.251 nm and 0.209 nm indexed to the (311) and (400) planes of cubic γ-Fe_2O_3. The results are in agreement with findings reported elsewhere [38,39]. As shown in Fig. 2 the nanoparticles look slightly bigger after conjugation around 19–22 nm diameters.

As expected, the hydrodynamic diameter of SPIONs was larger due to the fact that the particle doublets, triplets and aggregates were measured in water. The uniformity and stability of nanoparticles was generally better for SPIONs-CA compared to SPIONs and SPIONs-CA-FA, as demonstrated by the polydispersity index (PDI) values. DLS analysis shows a greater hydrodynamic diameter and wider agglomerates distribution of SPIONs (60.95 nm, PDI, 0.255) compared to those of the SPIONs-CA (60.08 nm, PDI, 0.165) while the hydrodynamic diameter was increased in FA conjugated SPIONs (72.54 nm, PDI, 0.176) due to the following: Bare iron oxide nanoparticles, without an appropriate surfactant or stabilizing polymer layer, have a hydrophobic surface which induces clustering in aqueous suspensions as they try to reduce their surface area in contact with water. SPIONs show tendency to lower the contact area with water by clustering against water due to the lack of a stabilizing polymer or a proper surfactant causing presence of a hydrophobic surface [40]. Moreover, potent attractive inter-molecular forces lead to clustering because of the particles wider size distribution. But then, SPIONs are coated via a shell of CA causing the reduction of attraction between the clusters. Also, DLS is remarkably sensitive to greater particles because it is highly dependent to aggregates scattered light intensity. In addition, reported average size is deviated due to scattering from relatively few but larger particle clusters; this clearly explains why the SPIONs-CA represent a size distribution in a narrower manner (polydispersity index of 0.165 compared to 0.255 for SPIONs) [41]. Then again, the average hydrodynamic diameter of SPIONs-CA-FA was heightened due to addition of FA to the surface and the thicker shell, but the PDI values did not remarkably increase (0.176), indicating that SPIONs-CA-FA kept its mono-dispersity and exhibited the narrow size distribution and stability of SPIONs. The stability of all the suspensions was also assessed via particle size measurement and PDI during storage at ambient conditions at 0, 1, 2 and 3 months.

The hydrodynamic diameters of SPIONs-CA and SPIONs-CA-FA did not significantly increase over the course of several months when stored at ambient temperature, which indicates good colloidal stability (Fig. 3).

Over time, PDI values were marginally changed although PDI values below 0.3 indicated fairly homogenous population of particles as well as no remarkable aggregation in the dispersion of nanoparticles over the course of storage. A repulsive barrier barricading aggregation of particles is formed due to the absorption of CA onto the surface of the

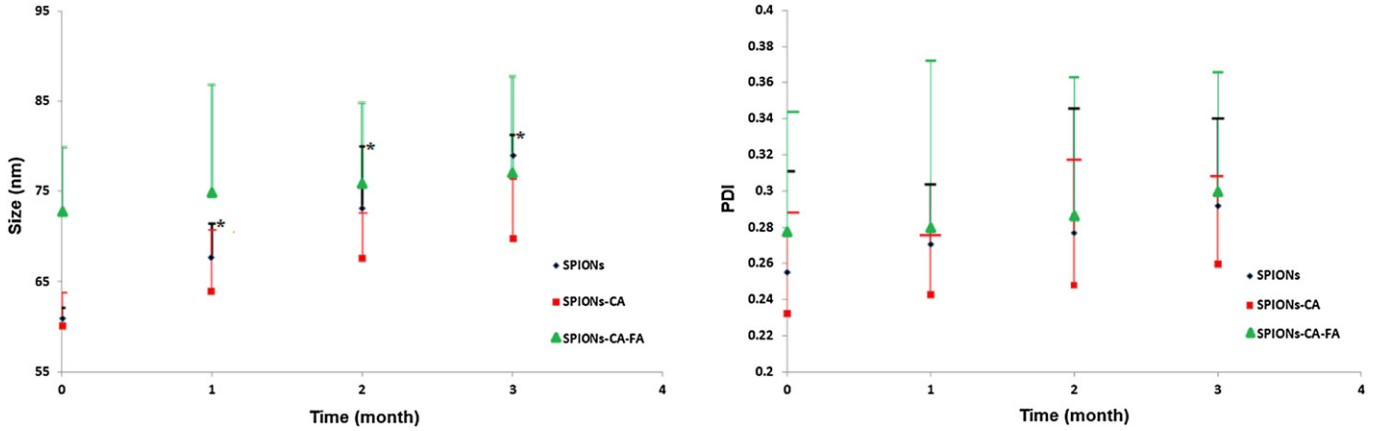

Fig. 3. The stability characteristics of SPIONs, SPIONs-CA and SPIONs-CA-FA in terms of mean hydrodynamic diameter (nm) (A) and polydispersity index (PDI) (B). Each value is the mean ± S.E.M. of six replicates. (*) indicates significant difference compared to the control analyzed by unpaired *t*-test followed by Holm-Sidak post hoc test ($p < 0.05$).

nanoparticles so that the stabilization effect of CA resulted in the stability of SPIONs-CA-FA [8,15].

XRD evaluated the phase purity and composition of the samples. Crystallinity of nanoparticles was confirmed by the presence of intense and sharp peaks. Fig. 4 shows the presence of diffraction peaks of γ-Fe_2O_3 at 2θ = 18.385, 30.245, 35.626, 43.300, 53.726, 57.275 and 62.901°, which correspond to the (111), (220), (311), (400), (422), (511), and (440) crystal planes of standard maghemite (γ-Fe_2O_3, JCPDS file no. 39-1346), and is identified to possess a cubic structure. Samples were identified as highly pure products because no other peaks were detected in the diffractogram. The X-ray diffraction pattern revealed highly crystalline nature formation of cubic structure of bare SPIONs and it was also retained after CA coating, only the peaks intensity slightly decreases. This fact shows that adsorption of CA on SPIONs does not change the crystalline structure of nanoparticles. The XRD pattern of SPIONs-CA nanoparticles showed similar pattern obtained elsewhere [15]. The X-ray diffraction pattern of SPIONs-CA-FA was similar to the SPIONs-CA along with additional characteristic peaks of folic acid at 30° [42]. The sharpness of the peaks represents highly crystalline nature of the initial γ-Fe_2O_3 that decreases in every functionalization step which is due to the existence of new materials on the surface of nanoparticles in each step. Hence, XRD and TEM results strongly inferred that the process yielded γ-Fe_2O_3 nanoparticles in pure phase.

Scherrer's formula was used to find the crystallite size with FWHM of peak 311 after correction for the instrumental broadening. The average crystallite size was found to be 8.2, 13.8 and 21.3 nm for SPIONs, SPIONs-CA and SPIONs-CA-FA respectively.

Generally, optimal drug delivery systems for systemic delivery are 10–100 nm in size however particles >200 nm and <10 nm are separated by the spleen or removed via clearance through kidneys, respectively [43,44]. Since the final synthesized SPIONs-CA-FA has an average size of 17 nm in this study, it indicates that stability of the product increased in physiological condition and the probability of elimination by the immune system decreased.

The surface chemical structure of the synthesized nanoparticles in each step was characterized using FTIR. The FTIR spectra analyses were displayed in Fig. 5. The adsorption peaks at around 500 to 600 cm^{-1} were related with the stretching and torsion vibration modes of the maghemite and the characteristic absorption of Fe—O bond which confirmed the existence of maghemite [45,46]. Presence of water traces and non-dissociated OH groups of citric acid is confirmed by existence of an intense band at 3400 cm^{-1}. Surface hydrolyzation of γ-Fe_2O_3 may infer the formation of $Fe(OH)_2$, $Fe(OH)_3$ and FeOOH [47]. The absorption bands for SPIONs-CA are broad and few while for pure CA are resolved. Existence of the peaks at 1623 and 1400 cm^{-1} confirmed the citric acid coating of the maghemite [48,49]. The 1730 cm^{-1} peak, assignable to the C═O vibration (symmetric stretching) from the COOH group in neat citric acid, after the binding of the citric acid to the maghemite surface, was shifted to a lower

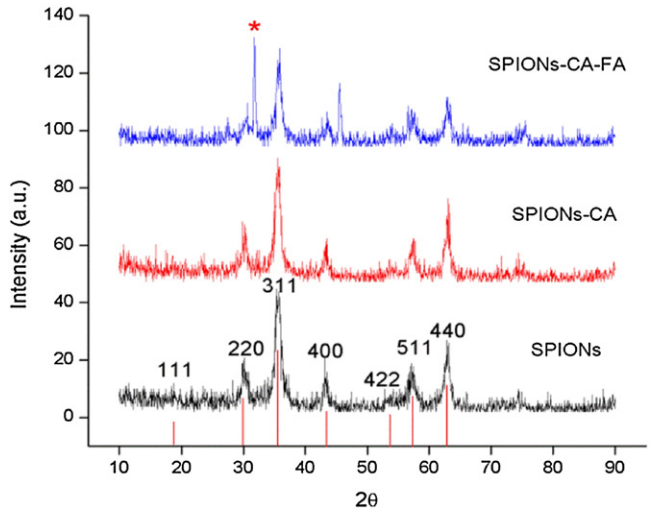

Fig. 4. XRD patterns of γ-Fe_2O_3, JCPDS file no. 39-1346 (show below), SPIONs, SPIONs-CA and SPIONs-CA-FA.

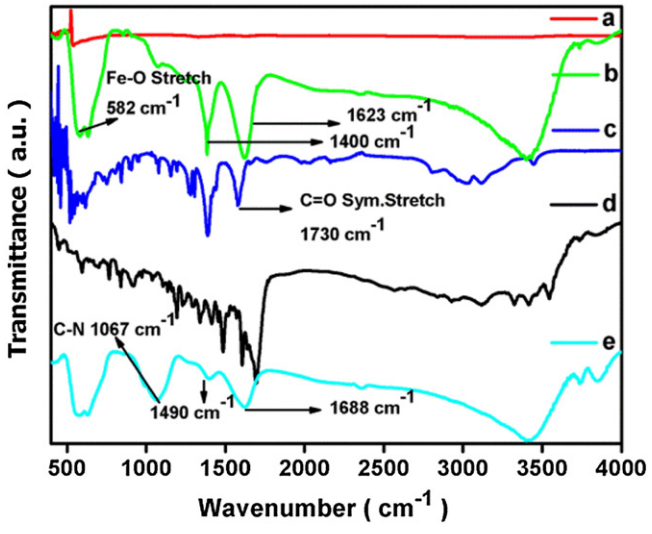

Fig. 5. FTIR spectrum of synthesized nanoparticles in each step. a) SPIONs, b) SPIONs-CA, c) CA, d) FA, e) SPIONs-CA-FA.

wave number. The neighbouring band at 1400 cm^{-1} was assigned to the asymmetric stretching of C═O [48,49]. It is suggested that carboxylate chemisorption helps CA to bind to the maghemite surface according to previous research studies [49,50].

In addition, FTIR peaks comparison before and after FA conjugation were used to confirm the existence of folic acid in SPIONs-CA-FA. Compared with SPIONs-CA, spectrum of SPIONs-CA-FA displays several new absorption peaks. During the conjugation by EDC/NHS click chemistry method the —COOH of SPIONs-CA was activated and then covalently attached to the —NH_2 of the FA, forming CO—NH band. Amide I band, C═O stretching, (~1688 cm^{-1}) and amide II band, N—H bending, (~1490 cm^{-1}) of the conjugates are much stronger than those of the neat FA, probably because of the formation of CO—NH by conjugation. Also the fingerprint absorption band of maghemite (~582 cm^{-1}) is observed for the conjugates, which shows that FA has been successfully conjugated to the SPIONs-CA [51]. The bands around 3690, 3739 and 3400 cm^{-1} are assigned to the stretch of the N—H bonds in the FA. This band could also represent O—H vibrations from trapped water molecules in the SPIONs-CA-FA [52]. Additionally, the out-of-plane and in-plane motions of (−NH_2) and (C—N) stretches of folic acid are attributed to the bands below 1700 cm^{-1}[53]. The presence of the stretching band C—N at (1067 cm^{-1}) was a remarkable fact confirming the covalent conjugation via amide linkage [50].

Total iron content in the SPIONs, SPIONs-CA and SPIONs-CA-FA was determined using AAS at 248.3 nm which were 19.98 g/l, 14.32 g/l and 4.566 g/l respectively. The ferrofluids at this concentration came into sight as a black liquid following magnet with no precipitation formed (Fig. 6). Despite rather high iron concentrations, the ferrofluids obtained in this study were stable during a period of several months at room temperature.

Fig. 6 shows the magnetization curves of synthesized nanoparticles, determined by VSM at room temperature. Higher amount of energy is required to demagnetize the SPIONs with larger area of their hysteresis loop [54]. In this research, the small area of hysteresis loop led to requirement of less amount energy for demagnetization [55]. The saturation magnetization (Ms) for SPIONs, SPIONs-CA and SPIONs-CA-FA were 69 emu/g, 58 emu/g and 21 emu/g of dried sample respectively. These values are confirmed with the values in the literature [56]. These results indicate that surface modification affected the magnetic properties. Magnetization value was decreased almost 32.9% between SPIONs and SPIONs-CA due to effect of particle size, higher surface disorder and the diamagnetic contributions of SPIONs-CA. A magnetization reduction of about 46.7% was observed between SPIONs-CA and SPIONs-CA-FA nanoparticles. Modifications in the structure of the particles could be the reason for the difference between these values. Covalent binding of FA to the carboxyl group of CA as well as increase in the inter-particle interactions are the reasons of structure change in particles throughout the modifications. The decrease was not remarkable as to seriously affect the use of product for the favorable applications. The level of Ms. obtained for SPIONs-CA-FA (21 emu/g) is adequate for such applications as Ms of 7–22 emu/g is accepted for biological applications [57,58]. On the other hand, consistency is seen between the linear decrease in Ms. of SPIONs, SPIONs-CA and SPIONs-CA-FA, and reduction in the magnetic content of SPIONs and conversely in organic content increase. The results are in agreement with literature [30] in which it was concluded that specific surface area and the specific saturation magnetization are inversely proportional. Therefore, the SPIONs can be easily separated from the solution using an external magnetic field because of superparamagnetism and large saturation magnetization values of the SPIONs. On the other point of view, successful CA coating and FA conjugation were confirmed by the decrease in saturation magnetization values.

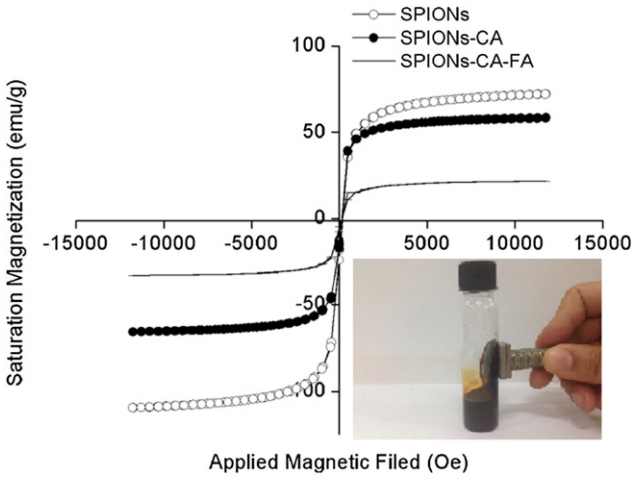

Fig. 6. Magnetization curves of synthesized nanoparticles.

3.2. Haemolysis; and in vitro RBC, WBC and PRP aggregation studies

Chemical composition and cellular components of blood would not be changed for at least 12 h *in vitro* if blood is heparinized as well as being preserved at room temperature [59,60]. Lysis of RBCs and release of heme into solution as effects of cytotoxic materials are detected by absorbance at 541 nm. In this study, the results of percentage haemolysis analysis do not show any signs of lysis when the particles are in contact with the erythrocytes in >200 μg/mL concentration in all cases (Table 1) and the percentage of lysis was found to be <1% which is well within the acceptable limits [61,62].

Fig. 7 exhibits the compatibility of the samples in terms of *in vitro* RBCs, WBCs and PRP aggregation. The images (Fig. 7) illustrate that the SPIONs-CA as well as the SPIONs-CA-FA behave similarly to the negative control (saline) and show no RBCs, WBCs and PRP aggregation or morphological change under the microscope in comparison with the positive control (Triton X-100) which may be attributed to the introduction of citric acid into the SPIONs. On the other hand, SPIONs showed slight aggregation and morphological change when incubated with RBCs, WBCs and PRP. Since the complex of constituents in vessel may affect the particle aggregation, a complete in vivo blood aggregation study is required to be carried out for further investigations.

These results confirmed the blood compatible nature of SPIONs-CA and SPIONs-CA-FA thus could be administrated intravenously to the blood stream safely during biomedical application. Hence the engineered SPIONs-CA-FA nanoparticle was found as a non-toxic material when in contact with blood.

However, the cytotoxicity of the SPIONs, SPIONs-CA and SPIONs-CA-FA were qualitatively determined using the colorimetric MTT assay on HSF 1184, MDA-MB-231, MDA-MB-468 and HeLa cell lines. The cells were incubated with 7.8, 15.62, 31.25, 62.5, 125, 250, 500 and 1000 μg Fe ml^{-1} of each SPIONs, SPIONs-CA and SPIONs-CA-FA for 24 h.

As shown in Fig. 8, after 24 h incubation with SPIONs-CA and SPIONs-CA-FA, the viability of all cell types are still >70% at all Fe

Table 1
Percentage of haemolysis of bare and modified SPIONs at three different concentrations.

Samples	Concentration (μg/m)	Haemolysis %
Triton X-100		100
Saline		0
SPIONs	100	0.321
	200	0.698
	300	1.831
SPIONs-CA	100	0.221
	200	0.436
	300	0.891
SPIONs-CA-FA	100	0.198
	200	0.521
	300	0.932

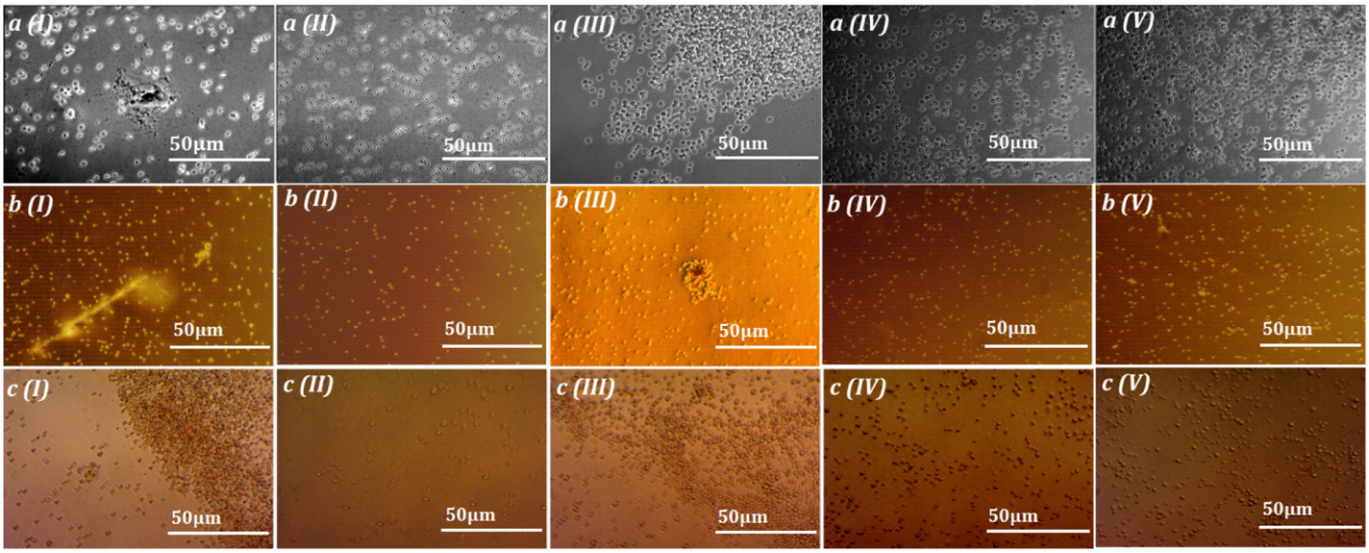

Fig. 7. Blood aggregation studies: a) RBCs incubated, b) PRP incubated and c) WBCs incubated with *(I)* +ve control, *(II)* −ve control, *(III)* SPIONs, *(IV)* SPIONs-CA, *(V)* SPIONs-CA-FA.

incubation concentrations. The result is in agreement with literature [63,64]. The SPIONs-CA and SPIONs-CA-FA showed >30% cell inhibition even at the highest concentration of 1000 μg/ml, but the viability of cells in the presence of SPIONs was lower in all cases representing that while SPIONs are slightly toxic to the cells, SPIONs-CA and SPIONs-CA-FA possess a reliable level of biocompatibility.

3.3. Binding study

In order to evaluate if SPIONs-CA-FA bind to the cancer cells *in vitro* in a selective manner, four different human cell lines were used: HSF 1184 (as normal skin human cell line not expressing folate receptors) [26], MDA-MB-231(as human breast cancer cells expressing folate

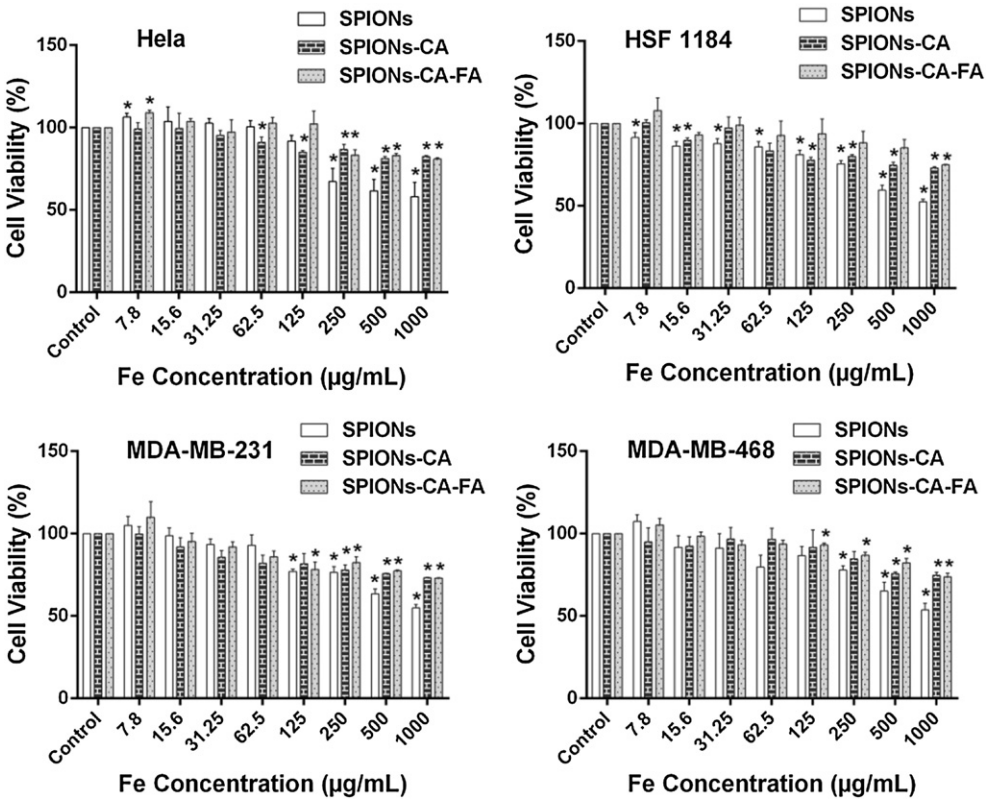

Fig. 8. MTT assay. Each value is the mean ± S.E.M. of six replicates out of three independent experiments. (*) indicates significant difference compared to the control analyzed by unpaired *t*-test followed by Holm-Sidak post hoc test ($p < 0.05$).

receptors) [65], MDA-MB-468 (as human breast cancer cells not expressing folate receptors) [66], HeLa (as human ovarian cancer cells overexpressing folate receptors) [53]. The quantitative analysis of iron uptake in different cells was performed by means of AAS. After treatment of each cell type with suspensions of SPIONs-CA and SPIONs-CA-FA in three different concentrations (100, 200 and 300 μg/ml) for 4, 12 and 24 h, mineralization of the cells were carried out and the iron content of cell lysates were measured based on the atomic absorbance of iron at 248.3 nm. The concentration of iron was below the detection limit compared to the control cells (Fig. 9).

A competitive binding assay was carried out to determine the dependence of cellular uptake on the folate receptors in FAR+ cells in the presence of 1 mM free folic acid which is necessary to restrict folate receptor-dependent binding in a competitive manner. 1 mM free folic acid remarkably decreased the cellular uptake (250 μg/ml for 24 h) in Hela and MDA-MB-231 cell lines while showed no significant effect on the decrement of SPIONs-CA-FA cellular uptake in HSF 1184 and MDA-MB-468 cell lines as represented in Fig. 10. The role that folate receptor pathway plays was revealed by the difference observed in the cellular uptake behaviour in Hela and MDA-MB-231 cell lines.

The internalization of SPIONs-CA and SPIONs-CA-FA at iron concentrations of 200 μg/ml were verified using Prussian blue staining method. Fig. 11 shows a large number of nanoparticles, the blue spots, within the cytoplasm of cells. The result gives an indication that the particles are mostly concentrated in the cytoplasm partially around the nucleus. There was a small uptake of iron after incubation with SPIONs-CA by endocytosis mechanism helping a variety of cells to passively take up the nanoparticles [67,68] while the active targeting of SPIONs-CA-FA increases the number of nanoparticles within FAR+ cancer cells (MDA-MB-231 and HeLa cell lines). However, the Prussian blue staining results confirm the AAS results in which more SPIONs-CA-FA are visualized as

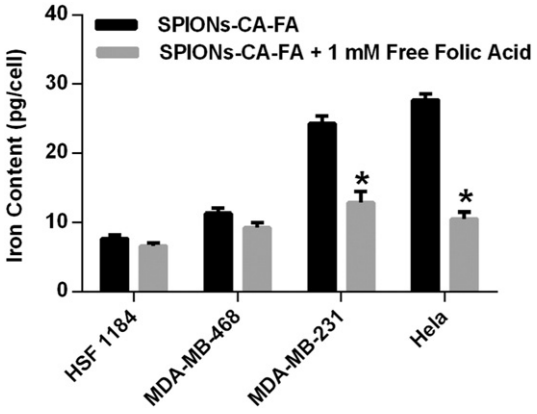

Fig. 10. Competitive binding assay. (*) indicates significant difference of uptake in presence of 1 mM free folic acid compared to the absence of 1 mM free folic acid ($p < 0.05$). Each value is the mean ± S.E.M. of six replicates.

blue spots on MDA-MB-231 (Fig. 11c *(III)*) and HeLa cells (Fig. 11b *(III)*) but less blue spots were visualized within HSF 1184, MDA-MB-468 cell lines. This assists the molecular recognition of folate overexpressing cancer cells. The results illustrated that SPIONs-CA-FA could be an ideal targeting candidate to the folate positive receptor cancers in biomedical application and it is worth for further investigations.

4. Conclusion

In summary, the CA coated superparamagnetic γ-Fe_2O_3 nanoparticles were successfully conjugated with FA via one-step surface alteration. The presented results exhibit that the surface of magnetite

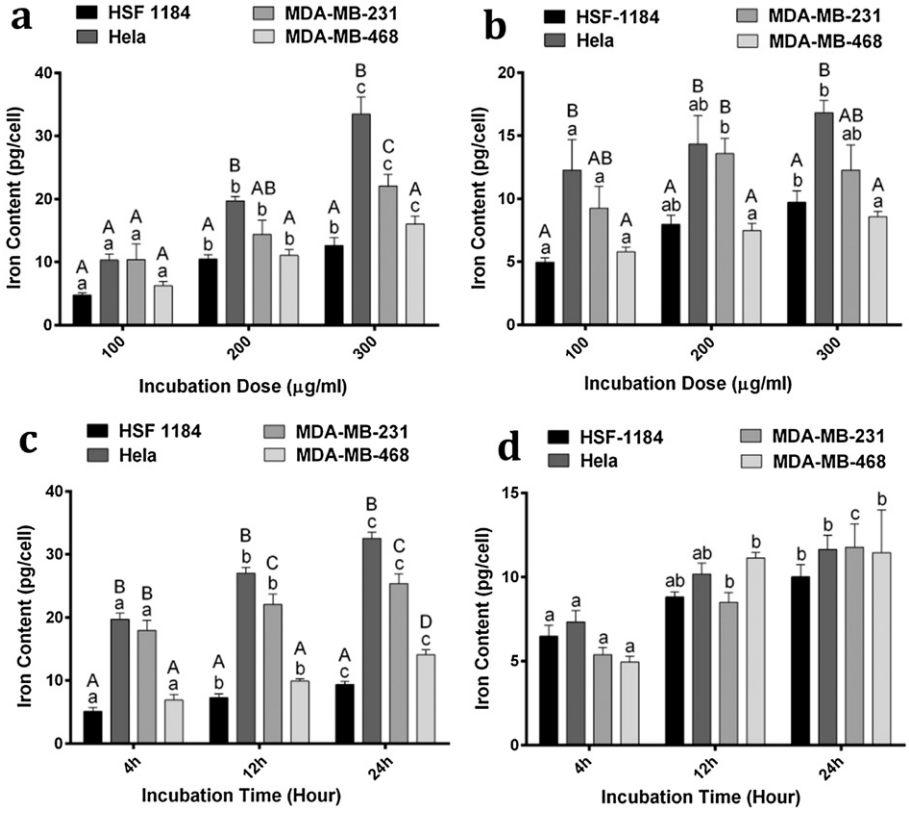

Fig. 9. Quantitative binding study, a) SPIONs-CA-FA treated for 24 h, b) SPIONs-CA treated for 24 h, c) SPIONs-CA-FA treated at 250 μg/ml, d) SPIONs-CA treated at 250 μg/ml (results are expressed as mean value ± S.E.M. from six independent experiments. Different capital letters depict significant differences between cell lines at a given incubation dose/time and lowercase letters depict significant differences for incubation dose/time effect on each particular cell line as determined by two-way ANOVA and Holm-Sidak post hoc multiple comparison test ($p < 0.05$).

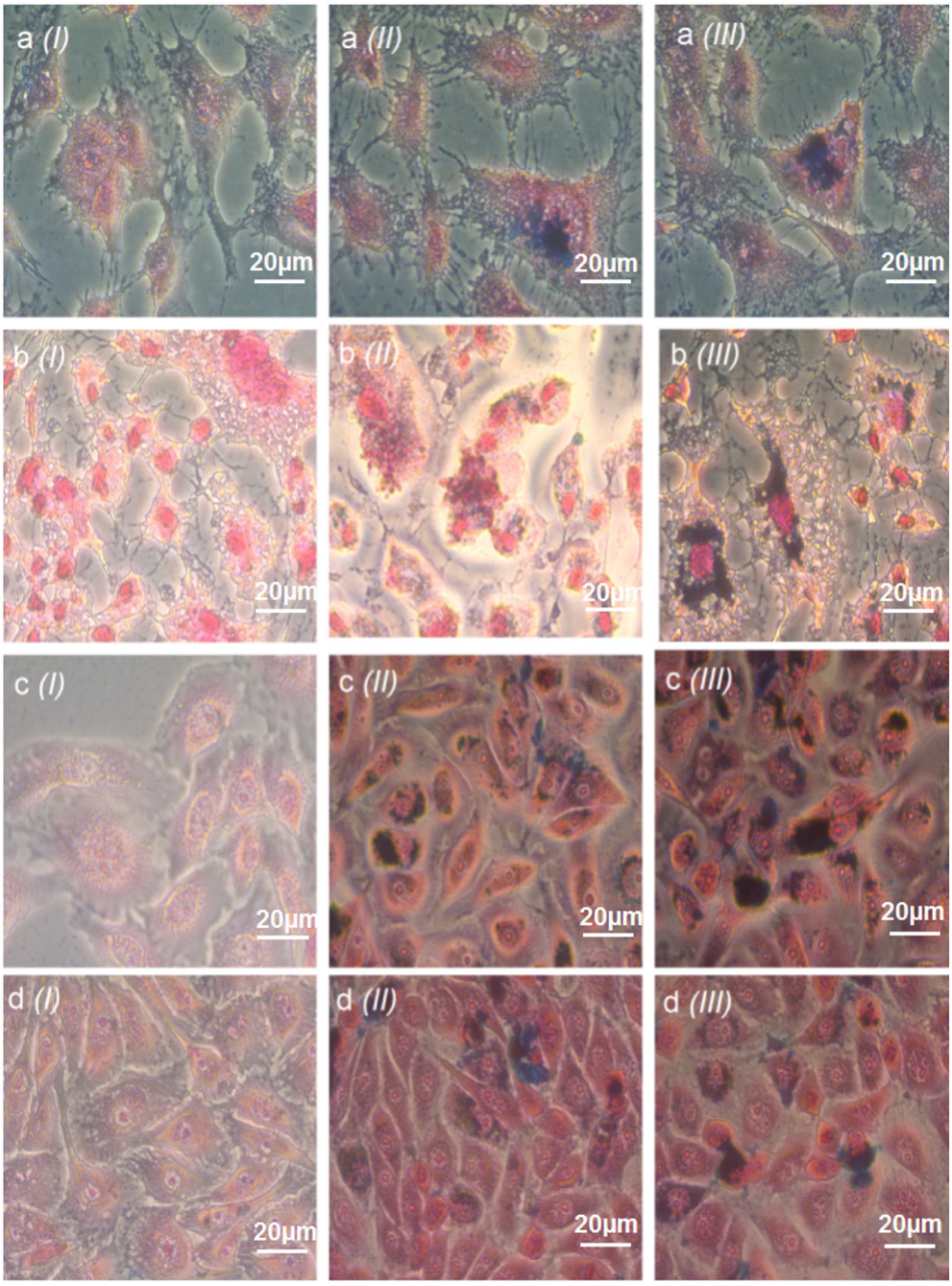

Fig. 11. Prussian blue stained images (a) HSF 1184 (b) HeLa cells (c) MDA-MB-231, d) MDA-MB-468, *(I)* non-treated, *(II)* SPIONs-CA treated and *(III)* SPIONs-CA-FA treated.

nanoparticles can be stabilized in an aqueous dispersion by the one-step adsorption of CA introducing reactive groups onto the surface of the SPIONs and making it biocompatible. The FA was effectively conjugated onto the surface of citric coated γ-Fe_2O_3 nanoparticles (50%) which was used as a targeting agent to the FAR+ cancer cells. The phase purity of final synthesized nanoparticles and its superparamagnetic properties (Ms of 21 emu/g) were confirmed using XRD diffractions pattern and VSM analysis respectively. Final engineered nanoparticle (SPIONs-CA-FA) possess adequate sizes, excellent biocompatibility, long lasting dispersibility and stability in aqueous solutions making this exquisite combination an attractive candidate for use in numerous areas of biomedical researches. The current results indicate that SPIONs-CA-FA are tolerated by HSF 1184, MDA-MB-468, MDA-MB-231 and HeLa cell lines and do not aggregate when exposed to RBCs, WBSs and PRP *in vitro*. Moreover, no haemolysis was observed when the cells were treated with different concentrations of SPIONs-CA-FA. As verified by Prussian blue staining and AAS analysis, the SPIONs-CA-FA exhibited better targeting and cellular internalization than did their non-targeted counterparts. Detection of early and metastatic cancer is eased up due to the high intracellular uptake of SPIONs-CA-FA compared with other conventional methods. Considering the unique and favorable properties of SPIONs-CA-FA, its applications may lead to the development of highly promising tool in bioingestion, magnetophoretic control, bioimaging, drug delivery, hyperthermia therapy and many other biomedical applications for FAR+ cancer cells.

Author contributions

The manuscript was written through contributions of all authors.

Notes

The authors declare no competing financial interest.

Acknowledgment

The authors would like to thank the Universiti Teknologi Malaysia for the financial support through Geran Universiti Penyelidikan (GUP) funding number Q.J130000.2524.06H09.

References

[1] S. Hu, M. Arellano, P. Boontheung, J. Wang, H. Zhou, J. Jiang, D. Elashoff, R. Wei, J.A. Loo, D.T. Wong, Salivary proteomics for oral cancer biomarker discovery, Clin. Cancer Res. 14 (19) (2008) 6246–6252.
[2] S.K. Singh, C. Hawkins, I.D. Clarke, J.A. Squire, J. Bayani, T. Hide, R.M. Henkelman, M.D. Cusimano, P.B. Dirks, Identification of human brain tumour initiating cells, Nature 432 (7015) (2004) 396–401.
[3] S. Laurent, D. Forge, M. Port, A. Roch, C. Robic, L. Vander Elst, R.N. Muller, Magnetic iron oxide nanoparticles: synthesis, stabilization, vectorization, physicochemical characterizations, and biological applications, Chem. Rev. 108 (6) (Jun. 2008) 2064–2110.
[4] C. Fang, M. Zhang, Multifunctional magnetic nanoparticles for medical imaging applications, J. Mater. Chem. 19 (35) (2009) 6258–6266.
[5] J.R. McCarthy, R. Weissleder, Multifunctional magnetic nanoparticles for targeted imaging and therapy, Adv. Drug Deliv. Rev. 60 (11) (2008) 1241–1251.
[6] K. Woo, J. Hong, S. Choi, H.-W. Lee, J.-P. Ahn, C.S. Kim, S.W. Lee, Easy synthesis and magnetic properties of iron oxide nanoparticles, Chem. Mater. 16 (14) (2004) 2814–2818.
[7] W. Wu, Q. He, C. Jiang, Magnetic iron oxide nanoparticles: synthesis and surface functionalization strategies, ChemInform 40 (24) (2009) i.
[8] L. Li, K.Y. Mak, C.W. Leung, K.Y. Chan, W.K. Chan, W. Zhong, P.W.T. Pong, Effect of synthesis conditions on the properties of citric-acid coated iron oxide nanoparticles, Microelectron. Eng. 110 (2013) 329–334.
[9] S.A. Wahajuddin, Superparamagnetic iron oxide nanoparticles: magnetic nanoplatforms as drug carriers, Int. J. Nanomedicine 7 (2012) 3445.
[10] T. Neuberger, B. Schöpf, H. Hofmann, M. Hofmann, B. Von Rechenberg, Superparamagnetic nanoparticles for biomedical applications: possibilities and limitations of a new drug delivery system, J. Magn. Magn. Mater. 293 (1) (2005) 483–496.
[11] C.P. Bean, J.D. Livingston, Superparamagnetism, J. Appl. Phys. 30 (4) (1959) S120–S129.
[12] M. Mahmoudi, A. Simchi, M. Imani, Recent advances in surface engineering of superparamagnetic iron oxide nanoparticles for biomedical applications, J. Iran. Chem. Soc. 7 (2) (2010) S1–S27.
[13] T.K. Jain, M.A. Morales, S.K. Sahoo, D.L. Leslie-Pelecky, V. Labhasetwar, Iron oxide nanoparticles for sustained delivery of anticancer agents, Mol. Pharm. 2 (3) (2005) 194–205.
[14] L. Vayssieres, C. Chanéac, E. Tronc, J.P. Jolivet, Size tailoring of magnetite particles formed by aqueous precipitation: an example of thermodynamic stability of nanometric oxide particles, J. Colloid Interface Sci. 205 (2) (1998) 205–212.
[15] S. Nigam, K.C. Barick, D. Bahadur, Development of citrate-stabilized Fe_3O_4 nanoparticles: conjugation and release of doxorubicin for therapeutic applications, J. Magn. Magn. Mater. 323 (2) (2011) 237–243.
[16] A. Lapresta-Fernández, T. Doussineau, S. Dutz, F. Steiniger, A.J. Moro, G.J. Mohr, Magnetic and fluorescent core–shell nanoparticles for ratiometric pH sensing, Nanotechnology 22 (41) (2011) 415501.
[17] C. Liu, P.M. Huang, Atomic force microscopy and surface characteristics of iron oxides formed in citrate solutions, Soil Sci. Soc. Am. J. 63 (1) (1999) 65–72.
[18] J.-H. Lee, Y.-M. Huh, Y. Jun, J. Seo, J. Jang, H.-T. Song, S. Kim, E.-J. Cho, H.-G. Yoon, J.-S. Suh, Artificially engineered magnetic nanoparticles for ultra-sensitive molecular imaging, Nat. Med. 13 (1) (2007) 95–99.
[19] G.F. Goya, V. Grazu, M.R. Ibarra, Magnetic nanoparticles for cancer therapy, Curr. Nanosci. 4 (1) (2008) 1–16.
[20] H. Choi, S.R. Choi, R. Zhou, H.F. Kung, I.-W. Chen, Iron oxide nanoparticles as magnetic resonance contrast agent for tumor imaging via folate receptor-targeted delivery 1, Acad. Radiol. 11 (9) (2004) 996–1004.
[21] D. Artemov, Molecular magnetic resonance imaging with targeted contrast agents, J. Cell. Biochem. 90 (3) (2003) 518–524.
[22] C. Leuschner, C.S.S.R. Kumar, W. Hansel, W. Soboyejo, J. Zhou, J. Hormes, LHRH-conjugated magnetic iron oxide nanoparticles for detection of breast cancer metastases, Breast Cancer Res. Treat. 99 (2) (Sep. 2006) 163–176.
[23] Y. Zhang, N. Kohler, M. Zhang, Surface modification of superparamagnetic magnetite nanoparticles and their intracellular uptake, Biomaterials 23 (7) (2002) 1553–1561.
[24] P. Garin-Chesa, I. Campbell, P.E. Saigo, J.L. Lewis Jr., L.J. Old, W.J. Rettig, Trophoblast and ovarian cancer antigen LK26. Sensitivity and specificity in immunopathology and molecular identification as a folate-binding protein, Am. J. Pathol. 142 (2) (1993) 557.
[25] J.F. Ross, P.K. Chaudhuri, M. Ratnam, Differential regulation of folate receptor isoforms in normal and malignant tissues in vivo and in established cell lines. Physiologic and clinical implications, Cancer 73 (9) (1994) 2432–2443.
[26] S.D. Weitman, R.H. Lark, L.R. Coney, D.W. Fort, V. Frasca, V.R. Zurawski, B.A. Kamen, Distribution of the folate receptor GP38 in normal and malignant cell lines and tissues, Cancer Res. 52 (12) (1992) 3396–3401.
[27] M. Barz, F. Canal, K. Koynov, R. Zentel, M.J. Vicent, Synthesis and in vitro evaluation of defined HPMA folate conjugates: influence of aggregation on folate receptor (FR) mediated cellular uptake, Biomacromolecules 11 (9) (2010) 2274–2282.
[28] R. Massart, Preparation of aqueous magnetic liquids in alkaline and acidic media, IEEE Trans. Magn. (1981) 1247–1248.
[29] A. Idris, N. Hassan, N. Suriani, M. Ismail, E. Misran, N. Mohd, A. Ngomsik, A. Bee, Photocatalytic magnetic separable beads for chromium (VI) reduction, Water Res. 44 (6) (2010) 1683–1688.
[30] A. Idris, N.S.M. Ismail, N. Hassan, E. Misran, A.-F. Ngomsik, Synthesis of magnetic alginate beads based on maghemite nanoparticles for Pb(II) removal in aqueous solution, J. Ind. Eng. Chem. 18 (5) (Sep. 2012) 1582–1589.
[31] N. Patel, M.C. Davies, M. Hartshorne, R.J. Heaton, C.J. Roberts, S.J.B. Tendler, P.M. Williams, Immobilization of protein molecules onto homogeneous and mixed carboxylate-terminated self-assembled monolayers, Langmuir 13 (24) (1997) 6485–6490.
[32] H. Wang, D.G. Castner, B.D. Ratner, S. Jiang, Probing the orientation of surface-immobilized immunoglobulin G by time-of-flight secondary ion mass spectrometry, Langmuir 20 (5) (2004) 1877–1887.
[33] C. Grüttner, K. Müller, J. Teller, F. Westphal, A. Foreman, R. Ivkov, Synthesis and antibody conjugation of magnetic nanoparticles with improved specific power absorption rates for alternating magnetic field cancer therapy, J. Magn. Magn. Mater. 311 (1) (2007) 181–186.
[34] E. Munnier, S. Cohen-Jonathan, K. Hervé, C. Linassier, M. Soucé, P. Dubois, I. Chourpa, Doxorubicin delivered to MCF-7 cancer cells by superparamagnetic iron oxide nanoparticles: effects on subcellular distribution and cytotoxicity, J. Nanopart. Res. 13 (3) (Oct. 2010) 959–971.
[35] A. Saraswathy, S.S. Nazeer, N. Nimi, S. Arumugam, S.J. Shenoy, R.S. Jayasree, Synthesis and characterization of dextran stabilized superparamagnetic iron oxide nanoparticles for in vivo MR imaging of liver fibrosis, Carbohydr. Polym. 101 (2014) 760–768.
[36] T. Mosmann, Rapid colorimetric assay for cellular growth and survival : application to proliferation and cytotoxicity assays, 65 (1983) 55–63.
[37] J.M. Saul, A. Annapragada, J.V. Natarajan, R.V. Bellamkonda, Controlled targeting of liposomal doxorubicin via the folate receptor in vitro, J. Control. Release 92 (1) (2003) 49–67.
[38] E. Matei, A. Predescu, E. Vasile, Properties of magnetic iron oxides used as materials for wastewater treatment, J. Phys. Conf. Ser. 304 (Jul. 2011) 012022.
[39] W. Cheng, K. Tang, Y. Qi, J. Sheng, Z. Liu, One-step synthesis of superparamagnetic monodisperse porous Fe_3O_4 hollow and core-shell spheres, J. Mater. Chem. 20 (9) (2010) 1799–1805.
[40] A. Kumar, M. Gupta, Synthesis and surface engineering of iron oxide nanoparticles for biomedical applications, 26 (2005) 3995–4021.
[41] S. Purushotham, R.V. Ramanujan, Thermoresponsive magnetic composite nanomaterials for multimodal cancer therapy, Acta Biomater. 6 (2) (Feb. 2010) 502–510.
[42] S.M. Haidary, E.P. Córcoles, N.K. Ali, Folic acid delivery device based on porous silicon nanoparticles synthesized by electrochemical etching, 8 (2013) 9956–9966.
[43] F. Alexis, E. Pridgen, L.K. Molnar, O.C. Farokhzad, Factors affecting the clearance and biodistribution of polymeric nanoparticles, 5 (4) (2008) 505–515 (Reviews).
[44] A. Manuscript, Clearance properties of nano-sized particles and molecules as imaging agents: considerations and caveats, Nanomedicine (Lond) 3 (5) (2012) 703–717.
[45] J.H. Almaki, R. Nasiri, A. Idris, F.A.A. Majid, M. Salouti, T.S. Wong, S. Dabagh, M. Marvibaigi, N. Amini, Synthesis, characterization and in vitro evaluation of exquisite targeting SPIONs–PEG–HER in HER2+ human breast cancer cells, Nanotechnology 27 (10) (2016) 105601.
[46] T.-Y. Juang, S.-J. Kan, Y.-Y. Chen, Y.-L. Tsai, M.-G. Lin, L.-L. Lin, Surface-functionalized hyperbranched poly(amido acid) magnetic nanocarriers for covalent immobilization of a bacterial γ-glutamyltranspeptidase, Molecules 19 (4) (Jan. 2014) 4997–5012.
[47] R. Kumar, Development and Potential Applications of Nanomaterials for Arsenic Removal From Contaminated Groundwater, March 2011.
[48] S. Nigam, K.C. Barick, D. Bahadur, Development of citrate-stabilized Fe_3O_4 nanoparticles: conjugation and release of doxorubicin for therapeutic applications, J. Magn. Magn. Mater. 323 (2) (Jan. 2011) 237–243.
[49] A. Airinei, Citric-acid – coated magnetite nanoparticles for biological applications, 121 (2006) 117–121.
[50] D.K. Bora, P. Deb, Fatty acid binding domain mediated conjugation of ultrafine magnetic nanoparticles with albumin protein, Nanoscale Res. Lett. 4 (2) (Jan. 2008) 138–143.
[51] Z. Wang, C. Zhou, J. Xia, B. Via, Y. Xia, F. Zhang, Y. Li, L. Xia, Colloids and surfaces B : biointerfaces fabrication and characterization of a triple functionalization of graphene oxide with Fe_3O_4, folic acid and doxorubicin as dual-targeted drug nanocarrier, Colloids Surf. B: Biointerfaces 106 (2013) 60–65.
[52] M.K. Ahmadi, M. Vossoughi, Immobilization of -chymotrypsin on the surface of magnetic/gold core/shell nanoparticles, 2013 (2013).
[53] G.A. Mansoori, K.S. Brandenburg, A. Shakeri-zadeh, A comparative study of two folate-conjugated gold nanoparticles for cancer nanotechnology applications, 7 (2010) 1911–1928.

[54] T. Wang, H. Wu, W. Wang, F. Lin, P. Lou, M. Shieh, T. Young, The development of magnetic degradable DP-Bioglass for hyperthermia cancer therapy, J. Biomed. Mater. Res. Part A 83 (3) (2007) 828–837.
[55] A. Tomitaka, T. Koshi, S. Hatsugai, T. Yamada, Y. Takemura, Magnetic characterization of surface-coated magnetic nanoparticles for biomedical application, J. Magn. Magn. Mater. 323 (10) (2011) 1398–1403.
[56] A. Idris, N. Suriani, M. Ismail, N. Hassan, E. Misran, A. Ngomsik, Journal of industrial and engineering chemistry synthesis of magnetic alginate beads based on maghemite nanoparticles for Pb (II) removal in aqueous solution, J. Ind. Eng. Chem. 18 (5) (2012) 1582–1589.
[57] N.A. Brusentsov, V.V. Gogosov, T.N. Brusentsova, A.V. Sergeev, N.Y. Jurchenko, A.A. Kuznetsov, O.A. Kuznetsov, L.I. Shumakov, Evaluation of ferromagnetic fluids and suspensions for the site-specific radiofrequency-induced hyperthermia of MX11 sarcoma cells in vitro, J. Magn. Magn. Mater. 225 (1) (2001) 113–117.
[58] C. Xu, K. Xu, H. Gu, X. Zhong, Z. Guo, R. Zheng, X. Zhang, B. Xu, Nitrilotriacetic acid-modified magnetic nanoparticles as a general agent to bind histidine-tagged proteins, J. Am. Chem. Soc. 126 (11) (2004) 3392–3393.
[59] G. Gokce, M. Citil, V. Gunes, G. Atalan, Effect of time delay and storage temperature on blood gas and acid–base values of bovine venous blood, Res. Vet. Sci. 76 (2) (2004) 121–127.
[60] A. Fura, T.W. Harper, H. Zhang, L. Fung, W.C. Shyu, Shift in pH of biological fluids during storage and processing: effect on bioanalysis, J. Pharm. Biomed. Anal. 32 (3) (2003) 513–522.
[61] A.C. Jayalekshmi, S.P. Victor, C.P. Sharma, Magnetic and degradable polymer/bioactive glass composite nanoparticles for biomedical applications, Colloids Surfaces B Biointerfaces 101 (2013) 196–204.
[62] C.V. Durgadas, K. Sreenivasan, C.P. Sharma, Bright blue emitting CuSe/ZnS/silica core/shell/shell quantum dots and their biocompatibility, Biomaterials 33 (27) (2012) 6420–6429.
[63] M. Szekeres, I.Y. Tóth, E. Illés, A. Hajdú, I. Zupkó, Chemical and colloidal stability of carboxylated core-shell magnetite nanoparticles designed for biomedical applications, 0067 (2013) 14550–14574.
[64] A.S.G. Ali, M.A. Reza, H. Eshghi, A. Sazgarnia, A.R. Montazerabadi, Cancerous Cells Targeting and Destruction Using Folate Conjugated Gold Nanoparticles, 2010.
[65] N. Nateghian, N. Goodarzi, M. Amini, F. Atyabi, M.R. Khorramizadeh, R. Dinarvand, Biotin/folate-decorated human serum albumin nanoparticles of docetaxel: comparison of chemically conjugated nanostructures and physically loaded nanoparticles for targeting of breast cancer, Chem. Biol. Drug Des. (2015).
[66] J. Varshosaz, S. Ghasemi, B. Behdadfar, Use of magnetic folate-dextran-retinoic acid micelles for dual targeting of doxorubicin in breast cancer, 2013 (2013).
[67] C.C. Berry, S. Wells, S. Charles, A.S.G. Curtis, Dextran and albumin derivatised iron oxide nanoparticles: influence on fibroblasts in vitro, Biomaterials 24 (25) (2003) 4551–4557.
[68] E.R.L. de Freitas, P.R.O. Soares, R. de Paula Santos, R.L. dos Santos, J.R. da Silva, E.P. Porfirio, S.N. Báo, L. de Oliveira, E. Celma, P.C. Morais, In vitro biological activities of anionic γ-Fe_2O_3 nanoparticles on human melanoma cells, J. Nanosci. Nanotechnol. 8 (5) (2008) 2385–2391.